Available online at www.sciencedirect.com
ScienceDirect
Ceramics International 34 (2008) 877–881
CERAMICS INTERNATIONAL
www.elsevier.com/locate/ceramint

Synthesis of nano-crystalline $Gd_{0.1}Ce_{0.9}O_{2-x}$ for IT-SOFC by aerosol flame deposition

Jong Mo Im, Hyun Jin You, Yong Sub Yoon, Dong Wook Shin *

Division of Materials Science & Engineering, Hanyang University, 17 Haengdang-dong, Seongdong-gu, Seoul 133-791, Republic of Korea

Available online 29 September 2007

Abstract

Nano-sized gadolinia-doped ceria (GDC) can be used as an IT-SOFC electrolyte, oxygen gas sensor or abrasives. In this study, nano-sized GDC powders with bimodal particle distribution of about 10 nm and 200 nm particle size were successfully synthesized by aerosol flame deposition (AFD). The resulting effects of sintering temperature on microstructure and electrical properties were investigated in the sintering temperature range 1100–1400 °C. The pellet had a completely dense microstructure after sintering at 1400 °C for 10 h. Raman measurement showed an increase of oxygen vacancy due to shift between reduced and oxidized states ($Ce^{3+} \leftrightarrow Ce^{4+}$) with increasing sintering temperature. The formation of oxygen vacancies noticeably increased the ionic conductivity above 1300 °C.

Keywords: B. Nanocomposites; D. CeO_2; Aerosol flame deposition (AFD)

1. Introduction

Ceria-based materials have been a candidate material for variety of potential applications due to their excellent electrochemical properties and material stability. Several rare-earth-doped cerium oxides exhibit high oxygen ionic conductivity, which makes them interesting materials for applications as solid oxide fuel cells (SOFCs) [1]. Cerium oxide has a fluorite structure stable up to its melting point, a large diffusion coefficient and good corrosion-resistance when compared with other pure oxides having oxygen ion conductivity. This material has also received attention as a stabilizer for ZrO_2, a glass-polishing medium, and an oxygen gas sensor [2,3]. Nanoparticles, in general, show higher catalytic activity, better sinterability, faster response time in sensor devices, better conductivity and other unusual properties in contrast to bulk materials [4]. If one tries to fabricate the ''micro'' or ''mini'' solid oxide fuel cell-based on the powder processes, it is essential to employ nano-sized powders since each components of the cell is constructed by thin films of various materials and their thicknesses are expected to be in the range of a few micrometers. Nano-powders are also preferable in terms of the electrochemical activities and interfacial contacts. The electrolyte layers composed of coarse particles generally require higher sintering temperature to eliminate open porosity [5]. However, higher sintering temperature may lead to unwanted interfacial reactions during co-sintering of electrolyte and cathode or anode layers and also results in the reduction of Ce^{4+} to Ce^{3+}, which contributes to electronic conduction [6]. To prepare electrolytes with lower sintering temperature, its particle size must be in the nanometer range. In the case of oxygen gas sensor, it has been reported that response time of the sensor-based on cerium oxide can be reduced by decreasing the particle size [7].

Traditional preparations of CeO_2 ultrafine particles involve include high-energy ball milling [6], co-precipitation [8], hydrothermal synthesis [9], sol–gel [10] and combustion synthesis [11]. Unlike these nanosized oxide powder techniques, aerosol flame deposition (AFD) process is unique since it offers a route to prepare both of nano-sized powders and nano-porous films under the ambient atmosphere. Compared with other wet-chemical methods mentioned, the advantages of this technique are a wide choice of nonvolatile precursors including liquid precursors, high degree of crystallinity of as-prepared metal oxide nanoparticles due to its high reaction temperatures (2000–3000 K), and the capability to produce virtually all kinds of oxide nano-sized powders that have been synthesized by solid state reactions [12].

* Corresponding author. Tel.: +82 2 2220 0503; fax: +82 2 2299 3851.
E-mail address: dwshin@hanyang.ac.kr (D.W. Shin).

0272-8842/$34.00
doi:10.1016/j.ceramint.2007.09.040

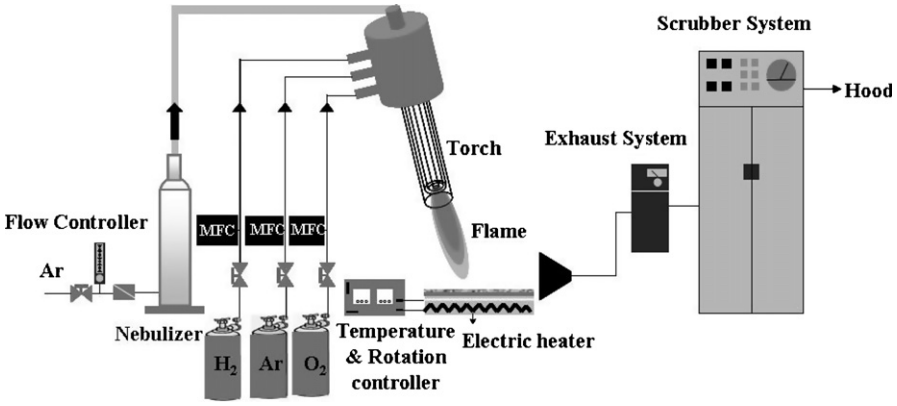

Fig. 1. A schematic diagram of aerosol flame deposition system for the synthesis of $Gd_{0.1}Ce_{0.9}O_{2-x}$.

In this paper, the aerosol flame deposition method was applied to synthesize nano-sized $Gd_{0.1}Ce_{0.9}O_{2-x}$ powders. The effects of synthesis and sintering temperature on the physical, chemical and electrical properties of $Gd_{0.1}Ce_{0.9}O_{2-x}$ powders were examined.

2. Experimental procedure

The experimental apparatus of AFD system is shown in Fig. 1. In the AFD process, a liquid precursor solution was prepared by dissolving the desired precursors into a solvent and then atomized into micro-sized droplets by ultrasonic nebulizer. The atomized droplets were carried by Ar carrier gas into a flame hydrolysis reaction zone in an oxy-hydrogen torch. The essential part of the system is the oxy-hydrogen torch, which is made from four concentric tubes creating three concentric gaps, and one shield tube keeping the flame stable. Precursor solution flows through the centermost tube of the torch while hydrogen, argon and oxygen flow through three gaps having different width to ensure laminar flow of gases. To prepare the solution, cerium nitrate hexahydrate, $Ce(NO_3)_3{\cdot}6H_2O$ (Aldrich, >99.9%) and gadolinium nitrate hexahydrate, $Gd(NO_3)_3{\cdot}6H_2O$ (Aldrich, >99.9%) were used as precursors and then ultrasonically agitated in methanol (CARLO ERBA, >95.0%) at room temperature to obtain a 0.05 M $Gd_{0.1}Ce_{0.9}O_{2-x}$ solution. The morphology and size of the GDC particles synthesized were characterized in plan-view using a scanning electron microscope (JEOL, JSM-6330F) and transmission electron microscope. The phase and crystallinity of the synthesized powders were investigated using an X-ray diffraction Rigaku M2500 diffractometer with a scanning step of 0.014°, a scanning time of 0.05 s per step and an angle range from 20° to 90°. Raman spectra were obtained using a Renishaw 2000 Raman spectromicroscope scanning from 200 cm^{-1} to 1000 cm^{-1} at room temperature in open-air. An Ar-ion laser beam with a wavelength of 514 nm was used to excite the nano-crystals. Impedance measurement of synthesized powders was carried out using a Solatron 1287 in combination with an impedance/gain-phase analyzer (Solatron 1260).

3. Results and discussion

The nano-sized and spherical $Gd_{0.1}Ce_{0.9}O_{2-x}$ particles were synthesized successfully by AFD and the color of the synthesized powder was light yellow. The powder color may be related to the variation of the particle size. Purohit et al. [4] also observed the light yellow color of the ceria powder with a particle size of about 10 nm. The as-prepared powder was composed of particles with two different size distributions. Smaller particles were approximately 10–20 nm in diameter and larger particles were approximately 100–200 nm in diameter, as shown in Fig. 2. The particles diameter distribution of $Gd_{0.1}Ce_{0.9}O_{2-x}$ particles revealed a bimodal size distribution, as shown in Fig. 2(B). The XRD pattern of synthesized powder, as shown in Fig. 3(A), exhibited the diffraction peaks of the ceria with a cubic structure and this suggests that a fully crystallized cubic phase gadolinium-doped ceria was successfully synthesized directly from the liquid precursor solution.

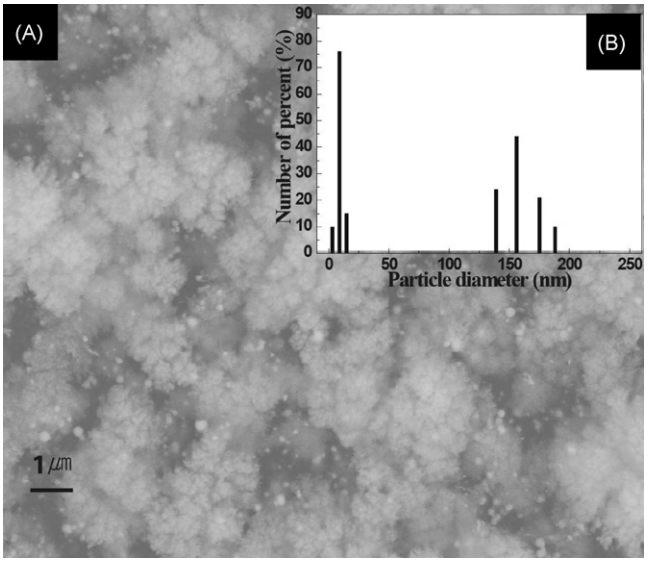

Fig. 2. SEM image and particle size distribution of $Gd_{0.1}Ce_{0.9}O_{2-x}$ powder synthesized at H_2 flow rate 3 l/min, O_2 flow rate 7.5 l/min, Ar flow rate 1 l/min, turn table temperature at 160 °C, precursor concentration 0.05 mol% on a Si wafer substrate.

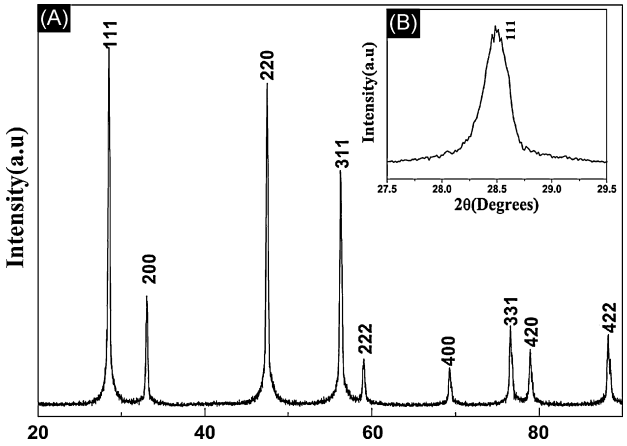

Fig. 3. XRD pattern of $Gd_{0.1}Ce_{0.9}O_{2-x}$ powder synthesized at H_2 flow rate 3 l/min, O_2 flow rate 7.5 l/min, Ar flow rate 1 l/min, turn table temperature at 160 °C, precursor concentration 0.05 mol% on Si wafer substrate. The peaks are indexed to the cubic structure of ceria. The inserted figure labeled to (B) is the detailed peak shape showing FWHM of (1 1 1) peak.

The crystallite size of the AFD-synthesized particle was calculated from full width at half maximum (FWHM) using Scherrer's formula, as shown in Fig. 3(B), for (1 1 1) crystal face of $Gd_{0.1}Ce_{0.9}O_{2-x}$ particles [13]. The particle diameter is given by

$$D = \frac{0.9\lambda}{\beta \cos\theta} \quad (1)$$

where D is the crystallite size in nm, λ the radiation wavelength (0.154056 nm in present case, Cu target), θ the diffraction angle, and β is the corrected line width at half peak intensity.

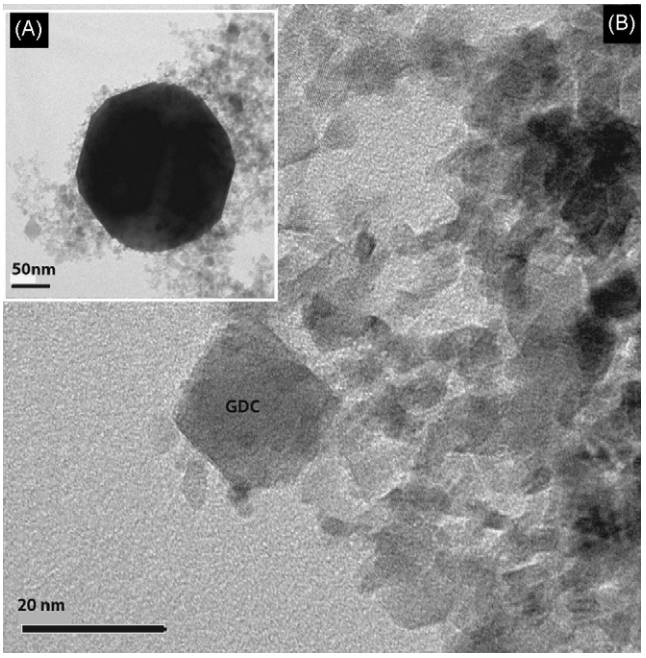

Fig. 4. TEM images of $Gd_{0.1}Ce_{0.9}O_{2-x}$ powder synthesized at H_2 flow rate 3 l/min, O_2 flow rate 7.5 l/min, Ar flow rate 1 l/min, turn table temperature at 160 °C, precursor concentration 0.05 mol% on Si wafer substrate.

β can be calculated using the formula:

$$\beta^2 = \beta_m^2 - \beta_s^2 \quad (2)$$

where β_m is the measured FWHM and β_s is the FWHM of a standard silicon sample (0.1704 [13]). Crystallite size of synthesized $Gd_{0.1}Ce_{0.9}O_{2-x}$ particles as calculated using Scher-

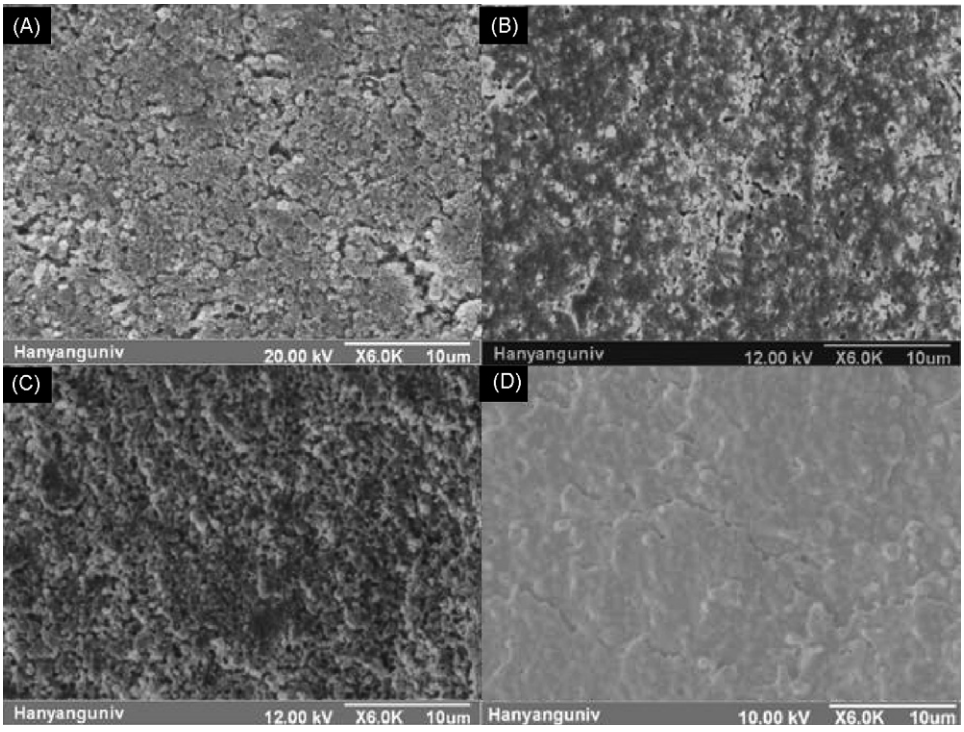

Fig. 5. SEM images of $Gd_{0.1}Ce_{0.9}O_{2-x}$ pellets sintered for 10 h at: (A) 1100 °C for 10 h, (B) 1200 °C for 10 h, (C) 1300 °C for 10 h and (D) 1400 °C.

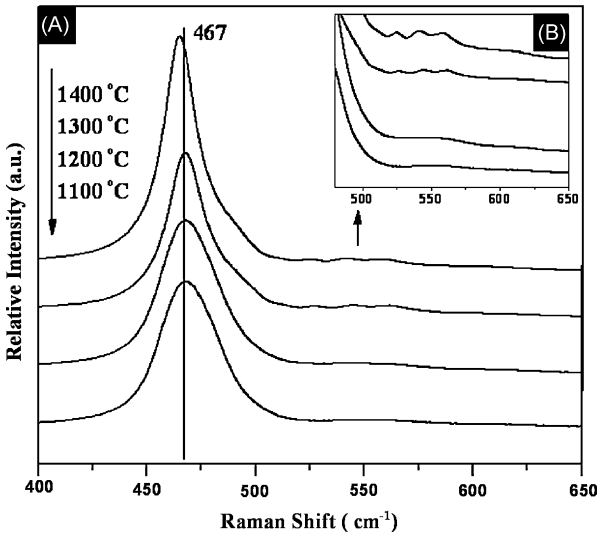

Fig. 6. Raman spectra of GDC samples sintered in the temperature range of 1100–1400 °C for 10 h. The inserted figure is a magnified spectra of oxygen vacancy.

rer's formula were 14.01 nm in diameter. The average primary particle could be also obtained from the TEM images of synthesized $Gd_{0.1}Ce_{0.9}O_{2-x}$ particles (Fig. 4) by averaging 20 particles and it was close to the calculated result (~20 nm).

The crystallite size of AFD-synthesized particle was slightly larger than that of other special synthesis processes such as co-precipitation [8] and combustion synthesis [11].

Fig. 5 shows the microstructure of pellets with $Gd_{0.1}Ce_{0.9}O_{2-x}$ particles at various sintering temperature from 1100 °C to 1400 °C. The open pores disappeared as the sintering temperature increased from 1100 °C to 1400 °C, and a moderately dense microstructure could be produced with a sintering temperature of 1400 °C for 10 h, as shown in Fig. 5(D). The film specimen was also fabricated and sintered at the same temperature, and the thickness of the sintered film was ~10 μm (the deposition rate was approximately 0.08 μm/min).

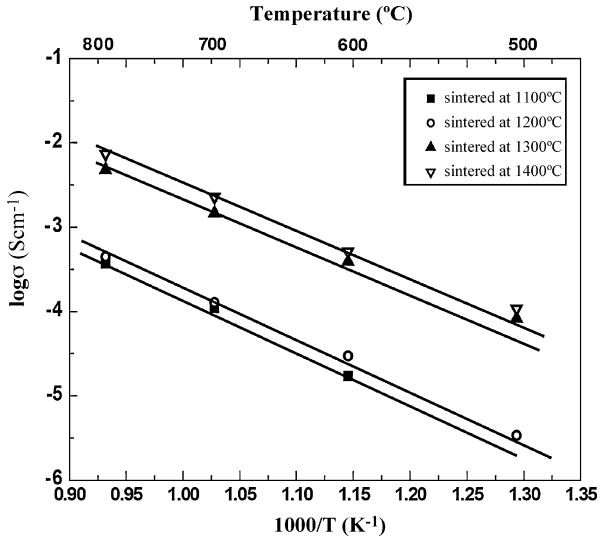

Fig. 7. Arrhenius plots for conductivities of the $Gd_{0.1}Ce_{0.9}O_{2-x}$ samples sintered in the temperature range of 1100–1400 °C for 10 h.

As presented in Fig. 6, the Raman spectrum of $Gd_{0.1}Ce_{0.9}O_{2-x}$ samples sintered in the temperature range of 1100–1400 °C shows typical spectra of $Ce_{1-x}RE_xO_{2-y}$ (RE = rare earth) solid solutions. Fluorite structure metal dioxides have only a single allowed Raman mode, which has F_{2g} symmetry and can be viewed as a symmetric breathing mode of the O atoms around each cation. The Raman band of $Gd_{0.1}Ce_{0.9}O_{2-x}$ samples appeared at 467 and near 560 cm^{-1}. As shown in Fig. 6(A), the peak at 467 cm^{-1} becomes sharp with increasing sintering temperature. The sharpening of the peak is attributed to the higher degree of cystallinity of $Gd_{0.1}Ce_{0.9}O_{2-x}$ solid solutions. Additionally, the peak weak shoulder on the high frequency side of the band near 560 cm^{-1} becomes perturbed. It is quiet clear that the intensity of the F_{2g} band increases with increasing sintering temperature. It is also known that the increase of sintering temperature results in the formation of oxygen vacancies, which perturb the local M–O band symmetry leading to the relaxation of symmetry selections [14]. The Arrhenius plots for conductivities of the sintered $Gd_{0.1}Ce_{0.9}O_{2-x}$ samples in air as a function of the inverse of temperature were measured as shown in Fig. 7. The data for the samples sintered at 1100 °C are compared with those for samples sintered at 1200°C, 1300°C and 1400 °C. From the data presented in Fig. 7, it is clearly shown that the conductivities of $Gd_{0.1}Ce_{0.9}O_{2-x}$ samples increase with increasing sintering temperature. Especially, the conductivity for the sample sintered at 1300 °C is about one order of magnitude larger than that of sample at 1200 °C and it was about 0.01 S cm^{-1}. Considering the result from the Raman spectra near 560 cm^{-1} reflecting the distortion of the O^{-2} sub-lattice in the CeO_2 lattice at high sintering temperature, it may be concluded that the abrupt increase in the conductivity is attributed to the increase of oxygen vacancies, which are responsible for the ionic conduction [15].

4. Conclusions

The nano-crystalline $Gd_{0.1}Ce_{0.9}O_{2-x}$ powder was synthesized by aerosol flame deposition technique. The synthesized particles were spherical, solid (dense), and free of agglomeration. The synthesized particles appeared to have a bimodal size distribution showing that smaller particles and larger particles were about 10 nm and 100 nm in an average diameter. It was observed that the displacement of the oxygen sublattice in the fluorite structure became greater with increase in sintering temperature, especially above a sintering temperature of 1300 °C. As a result of the oxygen vacancy concentration, the ionic conductivity increased appreciably above 1300 °C.

In this study, it was demonstrated that aerosol flame deposition is one of the satisfactory process technique for the production of nano-size crystalline $Gd_{0.1}Ce_{0.9}O_{2-x}$ powder and film.

References

[1] S. Zha, C. Xia, G. Meng, Effect of Gd (Sm) doping on properties of ceria electrolyte for solid oxide fuel cells, J. Power Sources 115 (2003) 44–48.
[2] M. Hirano, E. Kato, Hydrothermal synthesis of nanocrystalline cerium(IV) oxide powders, J. Am. Ceram. Soc. 82 (1999) 786–788.

[3] K.R. Reddy, K. Karan, Sinterability, mechnical, microstructural, and electrical properties of gadolinium-doped ceria electrolyte for low-temperature solid oxide fuel cells, J. Electroceram. 15 (2005) 45–56.
[4] R.D. Purohit, S. Saha, A.K. Tyagi, Powder characteristics and sinterability of ceria powders prepared through different routes, Ceram. Int. 32 (2006) 143–146.
[5] T.S. Zhang, J. Ma, Y.J. Leng, S.H. Chan, Effect of transition metal oxides on densification and electrical properties of Si-containing $Ce_{0.8}Gd_{0.2}O_{2-x}$ ceramics, Solid State Ionics 168 (2004) 187–195.
[6] R.S. Torrens, N.M. Sammes, G.A. Tompsett, Characterisation of $(CeO_2)_{0.8}(GdO_{1.5})_{0.2}$ synthesised using various techniques, Solid State Ionics 111 (1998) 9–15.
[7] N. Izu, W. Shin, I. Matsubara, N. Murayama, Development of resistive oxygen sensors-based on cerium oxide thick film, J. Electroceram. 13 (2004) 703–706.
[8] X. Yu, F. Li, X. Ye, X. Xin, Synthesis of cerium(IV) oxide ultrafine particle by solid-state reactions, J. Am. Ceram. Soc. 83 (2004) 964–966.
[9] K. Yamashita, K.V. Ramanujachary, M. Greenblat, Hydrothermal synthesis and low temperature conduction properties of substituted ceria ceramics, Solid State Ionics 81 (1995) 53–60.
[10] M. Thammachart, V. Meeyoo, T. Risksomboon, S. Osuwan, Catalytic activity of CeO_2–ZrO_2 mixed oxide catalysts prepared via sol–gel technique: CO oxidation, Catal. Today 68 (2001) 53–61.
[11] R.D. Purohit, B.P. Sharma, K.T. Pillai, A.K. Tyagi, Ultrafine ceria powders via glycine–nitrate combustion, Mater. Res. Bull. 36 (2001) 2711–2721.
[12] K.H. Cho, D.W. Shin, Fabrication of Li_2O–B_2O_3–P_2O_5 solid electrolyte by flame-assisted ultrasonic spray hydrolysis for thin film battery, Electrochim. Acta 52 (2006) 1571–1575.
[13] T. Mahata, G. Das, R.K. Mishra, B.P. Sharma, Combustion synthesis of gadolinia-doped ceria powder, J. Alloy Compd. 391 (2005) 129–135.
[14] J.R. McBride, K.C. Hass, B.D. Poindexter, W.H. Weber, Raman and X-ray studies of $Ce_{1-x}RE_xO_{2-y}$, where RE = La, Pr, Nd, Eu, Gd and Tb, J. Appl. Phys. 76 (1994) 2435–2441.
[15] I. Hideaki, T. Hiroaki, Ceria-based solid electrolyte, Solid State Ionics 83 (1996) 1–16.